

Magnetically stable zero-bias anomaly in Andreev contact to the magnetic Weyl semimetal $\text{Co}_3\text{Sn}_2\text{S}_2$

O.O. Shvetsov, Yu.S. Barash, S.V. Egorov, A.V. Timonina, N.N. Kolesnikov, and E.V. Deviatov

*Institute of Solid State Physics of the Russian Academy of Sciences,
Chernogolovka, Moscow District, 2 Academician Ossipyan Str., 142432 Russia*

(Dated: February 15, 2021)

Being encouraged by the interplay between topology, superconductivity and magnetism, we experimentally investigate charge transport through the interface between the Nb superconductor and the time-reversal symmetry breaking Weyl semimetal $\text{Co}_3\text{Sn}_2\text{S}_2$. In addition to the proximity induced superconducting gap, we observe several subgap features, among which the most interesting is the prominent subgap zero-bias anomaly, absolutely stable against external magnetic fields up to the critical field of Nb. As the promising scenario for the zero-bias anomaly to appear in transport characteristics, we consider the proximity induced zero-energy Andreev bound states interfaced with the half-metallic $\text{Co}_3\text{Sn}_2\text{S}_2$ and influenced by the strong spin-orbit coupling and large Zeeman splitting.

PACS numbers: 73.40.Qv 71.30.+h

I. INTRODUCTION

A magnetic Weyl semimetal (WSM) with broken time-reversal symmetry can be interpreted as a 3D heterostructure consisting of the layers of Chern insulators¹. For WSM, the coupling between the layers closes the bulk band gap at isolated points of the Brillouin zone. These band touching points with linear dispersion, also called Weyl nodes, are topological objects^{2,3}. Their topological protection is guaranteed by a non-zero Chern number defined on a sphere in momentum space enclosing a given Weyl node.

In transport studies, an anomalous Hall effect (AHE) is the hallmark of a WSM phase⁴. AHE originates from the topologically protected chiral surface states residing in the Fermi arcs, which connect projections of Weyl nodes on the surface Brillouin zone and inherit the chiral property of Chern insulator edge states^{2,3}. The Fermi-arc states can play an important role in forming the transport properties of WSM not only when the bulk contribution is strongly suppressed or absent for a special reason, as in AHE. The anomalous contribution to a number of transport coefficients from the Fermi arcs can be of the same order as from the bulk states even in large systems⁵.

Physics becomes even more exciting if one considers a magnetic WSM in proximity to an *s*-wave spin-singlet superconductor. The unusual band structure of WSM and its nontrivial topological properties modify Andreev reflection processes and result in new proximity-induced effects as compared to what was known until recently⁶⁻¹³. A variety of possible superconducting phases with and without Weyl points, that can possess distinct topological features depending on the Zeeman splitting strength and the magnitude of the proximity effect, have been theoretically identified within the BCS-like model in magnetic WSM films¹⁴. In this case the superconductivity splits each electronic state into a particle-hole symmetric and antisymmetric states. Correspondingly, the system does not generally develop a superconducting gap, but splits

each Weyl node of a given chirality into two separated Bogoliubov-Weyl nodes with opposite particle-hole symmetry. The particle-hole symmetric and antisymmetric subspaces are decoupled and the Majorana bound states can eventually emerge at the WSM surface. On the other hand, conventional Andreev reflection should be suppressed for the bulk excitations near a certain Weyl node due to chirality blockade¹⁵: a change in chirality is required in order to preserve spin-singlet pairing with its transfer of zero-spin and zero-momentum. When the proximity-induced superconductivity in the bulk is substantially suppressed, the superconductivity in the Fermi arcs has been predicted to show up and, in the simplest cases, found to emerge as a pure triplet state or a singlet-triplet mixture¹⁶. The appearance of chiral zero-energy Majorana bound states has been identified for the triplet pairing. Thus, topologically protected surface states of WSM form a potential platform for realization of chiral Majorana bound states².

There are only a few candidates of time-reversal symmetry breaking WSMs^{3,17-19}. Recently, the giant AHE has been reported^{20,21} for the kagome-lattice half-metallic ferromagnet $\text{Co}_3\text{Sn}_2\text{S}_2$ as an anomalous Hall conductance in zero magnetic field. The existence of Fermi arc surface states in the material was confirmed by angle-resolved photoemission spectroscopy^{21,22} and scanning tunneling microscopy²³. The magnetic moments of cobalt become ferromagnetically ordered out of kagome-lattice Co_3Sn planes below 175K. The Co planes are interleaved with buffer planes of triangularly ordered tin and sulfur. Though the bulk-edge correspondence generally relates the topological invariants in the bulk to the topologically protected surface arcs, specific connectivities among the Weyl nodes and the corresponding STM/STS spectra turn out to be not generally predetermined and can be associated with the particular Sn-, S-, or Co- surface terminations^{23,24}.

Here, we experimentally investigate charge transport through the interface between a Nb superconductor and

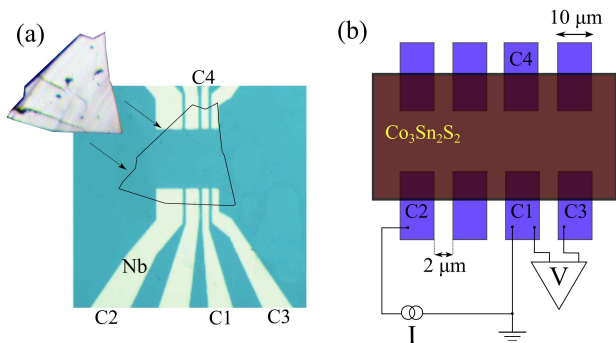


FIG. 1. (Color online) (a) The top-view image of the sample. A flat $\text{Co}_3\text{Sn}_2\text{S}_2$ single crystal (about $100 \mu\text{m}$ size and $1 \mu\text{m}$ thick) is transferred on top of the Nb leads, preliminary defined on a SiO_2 substrate. Planar junctions are formed with $\approx 10 \mu\text{m}$ overlap. (b) The sketch of a sample with the circuit diagram. The distance between the leads is $2 \mu\text{m}$. Charge transport is investigated with a standard three-point technique: the studied contact (C1) is grounded and the two other contacts (C2 and C3) are used for applying current and measuring potential.

a magnetic WSM $\text{Co}_3\text{Sn}_2\text{S}_2$. Aside from Andreev reflection, we observe several additional features, among which the most impressive is the prominent zero-bias anomaly (ZBA), fairly stable against external magnetic fields up to the critical field of Nb. We discuss possible scenarios that could result in magnetically stable ZBA under the conditions studied, taking into account the topological nature of WSM and its interfaces as well as the presence of the spin-orbit coupling and large Zeeman splitting, which are intrinsic for the half-metallic WSM.

II. SAMPLES AND TECHNIQUE

$\text{Co}_3\text{Sn}_2\text{S}_2$ single crystals were grown by the gradient freezing method. An initial load of high-purity elements taken in stoichiometric ratio was slowly heated up to 920°C in the horizontally positioned evacuated silica ampule, held for 20 h and then cooled with the furnace to ambient temperature at the rate of 20 deg/h . The obtained ingot was cleaved in the middle part. The Laue patterns confirm the hexagonal structure with (0001) as a cleavage plane. Electron probe microanalysis of cleaved surfaces and x-ray diffractometry of powdered samples confirmed the stoichiometric composition of the crystal.

The kagome-lattice ferromagnet $\text{Co}_3\text{Sn}_2\text{S}_2$ has the (0001) cleavage plane, but bonds between the layers in the crystal are quite strong. Thin flakes of $\text{Co}_3\text{Sn}_2\text{S}_2$ can not be easily mechanically exfoliated, e.g., with a scotch-tape technique. Thus, only rather thick flakes (about $100 \mu\text{m}$ size and $1 \mu\text{m}$ thick) can be exfoliated by rough mechanical cleavage. We selected the flattest flakes with a clean surface, which was verified by an optical microscope.

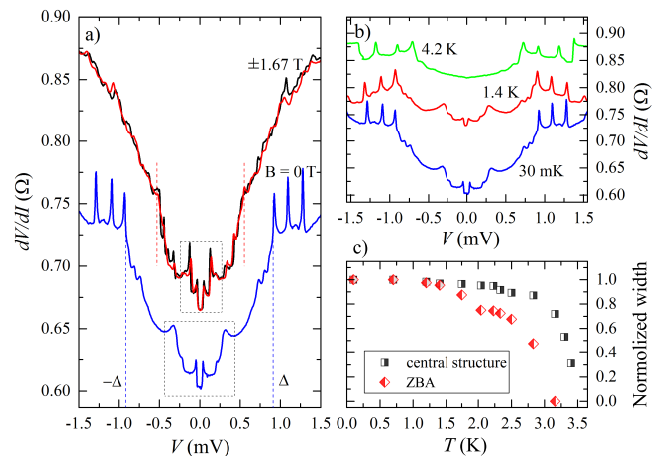


FIG. 2. (Color online) $dV/dI(V)$ characteristics in different conditions for one of the Nb- $\text{Co}_3\text{Sn}_2\text{S}_2$ junctions. (a) $dV/dI(V)$ curves are measured at 30 mK. External magnetic field B is zero for the blue curve, and equal to $\pm 1.67 \text{ T}$ for the black and red curves, respectively. The superconducting gap, marked by the blue (zero field) and red ($\pm 1.67 \text{ T}$) dashed lines, is suppressed in magnetic fields. The subgap structure is marked by the black dashed rectangle, it is diminishing proportionally to the superconducting gap in magnetic fields. ZBA, on the contrary, is robust against magnetic fields. Magnetic field is normal to the sample's plane. (b) $dV/dI(V)$ characteristics of the same junction at different temperatures. ZBA is suppressed by temperature, while the proximity induced superconducting gap is still observable. The curves are shifted for clarity both in (a) and (b). (c) Normalized width of the subgap structure (the black rectangles) and ZBA (the red diamonds) versus temperature.

Then, a small $\text{Co}_3\text{Sn}_2\text{S}_2$ flake is transferred to the Nb leads pattern, see Fig. 1 (a). The leads pattern is defined on an insulating SiO_2 substrate by a lift-off technique after magnetron sputtering of 150 nm Nb. The leads are separated by $2 \mu\text{m}$ intervals. Further, a $\text{Co}_3\text{Sn}_2\text{S}_2$ flake is pressed to the leads slightly with another oxidized silicon substrate. A weak pressure is applied with a special metallic frame, which keeps the substrates strictly parallel. This procedure provides transparent contacts, stable in different cooling cycles, without mechanical polishing or chemical treatment^{25–27}.

It has been shown previously, that our samples demonstrate a giant AHE²⁷, which is a hallmark of $\text{Co}_3\text{Sn}_2\text{S}_2$ Weyl semimetal^{20,21}. The bulk of the samples is fully spin-polarized²⁷ above 0.5 T .

A standard three-point technique is used to study electron transport across a single Nb- $\text{Co}_3\text{Sn}_2\text{S}_2$ junction, see Fig. 1(b): one Nb contact (C1) is grounded and two other contacts are used for applying current (C2) and measuring potential (C3). To obtain $dV/dI(V)$ characteristics, dc current is additionally modulated by a low (below $5 \mu\text{A}$, $f \approx 1 \text{ kHz}$) ac component. We measure both dc (V) and ac ($\sim dV/dI$) components of the potential with a dc voltmeter and a lock-in, respectively, after

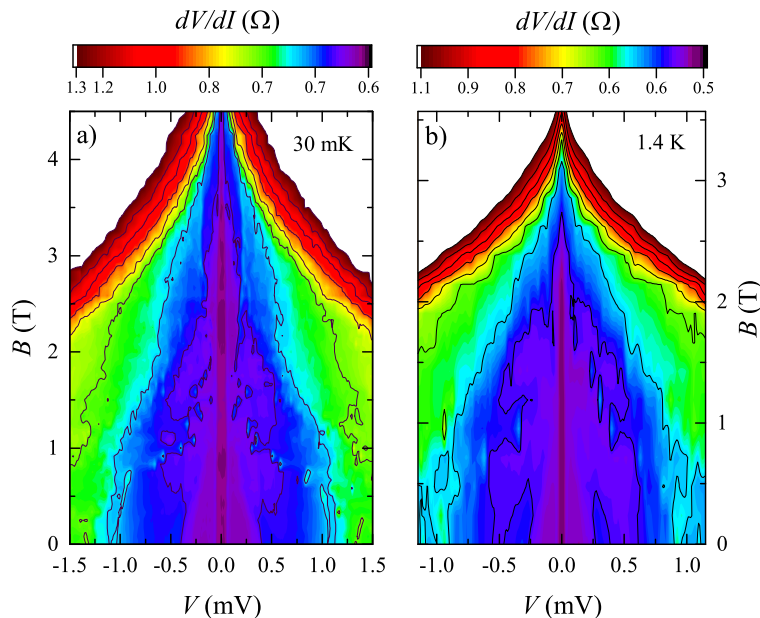


FIG. 3. (Color online) Evolution of $dV/dI(V)$ characteristic of the Nb- $\text{Co}_3\text{Sn}_2\text{S}_2$ junction in magnetic fields (a) at $T = 30$ mK and (b) at $T = 1.4$ K. At both temperatures, ZBA (the violet stripe around zero bias) is stable against magnetic fields. Suppression of ZBA starts only close to the critical field of the superconducting gap.

a broad-band preamplifier. We checked that the lock-in signal is independent of the modulation frequency. The obtained $dV/dI(V)$ characteristics are verified to be independent of mutual positions of current/voltage probes (e.g., changing C2 to C4 or C3 to C4 in Fig. 1(b)), so they reflect transport parameters of the Nb- $\text{Co}_3\text{Sn}_2\text{S}_2$ interface without admixtures of the sample's bulk resistance. We also checked that $dV/dI(V)$ characteristics are well reproducible in different cooling cycles. The measurements are performed in a dilution refrigerator (30 mK - 1.2 K) and in a usual He^4 cryostat (1.4 K - 4.2 K).

III. EXPERIMENTAL RESULTS

The blue curve in Fig. 2 demonstrates $dV/dI(V)$ characteristic of the Nb- $\text{Co}_3\text{Sn}_2\text{S}_2$ junction at the lowest temperature 30 mK and zero external magnetic field. The overall behavior of the curve is consistent with the known one for a single Andreev contact to a ferromagnet²⁸: niobium superconducting gap is observed as a dV/dI drop and denoted by the blue dashed lines. The gap $\Delta = 0.9$ meV is the Nb gap suppressed by the ferromagnetism of the $\text{Co}_3\text{Sn}_2\text{S}_2$ flake in a vicinity of the interface by 40%, as compared to the Nb gap in the bulk $\Delta_{\text{Nb}} = 1.5$ meV. Such a suppression could indicate to a large spin-mixing angle acquired by the quasiparticles in the reflection and/or transmission interface processes^{29,30}. As the subgap resistance is lower than the normal one, one may assume that we have a transparent Nb- $\text{Co}_3\text{Sn}_2\text{S}_2$ interface. Although the interface quality allows us to ob-

serve the Andreev physics in the Nb- $\text{Co}_3\text{Sn}_2\text{S}_2$ junctions, it prevents the proximity-induced Josephson current³¹ to flow across the WSM $\text{Co}_3\text{Sn}_2\text{S}_2$ connecting 2 μm spaced superconducting Nb contacts, irrespective of the presence or absence of the applied external magnetic field.

In addition to the Nb superconducting gap, the blue curve at zero magnetic field and 30 mK in Fig. 2(a) demonstrates several features both inside and outside the gap. There are sharp periodic peaks outside the Nb gap, which are likely to be geometrical resonances, known for Andreev contacts³²⁻³⁴. Also, there is a wide (± 0.45 meV width) central structure, which is denoted by the dashed rectangle in Fig. 2(a) and can be understood³⁵⁻³⁷ as the proximity induced soft³⁸ superconducting gap Δ_S at the surface of $\text{Co}_3\text{Sn}_2\text{S}_2$. The gap Δ_S has approximately the BCS-like temperature dependence⁷ and nearly satisfies the BCS relation $\Delta_S \approx 1.76k_B T_{cS}$, where $T_{cS} = 3.5$ K in Fig. 2(c) and $\Delta_S = 0.45$ meV in Fig. 2(a).

In the center of the subgap structure ZBA appears as a narrow (± 0.06 meV width) dV/dI drop. Our most notable result is that ZBA exhibits absolute robustness to external magnetic fields, which is demonstrated in Fig. 2(a), see the black and red curves at ± 1.67 T. The resonances outside the gap disappear under the magnetic field, while the subgap structure region, denoted by the black dashed rectangle in Fig. 2(a), diminishes proportionally to the superconducting gap in the field. This behavior is independent on the field's sign; compare the black (+1.67 T) and red (-1.67 T) curves in Fig. 2(a).

In contrast to the magnetic field, an increase in temperature has a dramatic influence on ZBA: it shrinks and

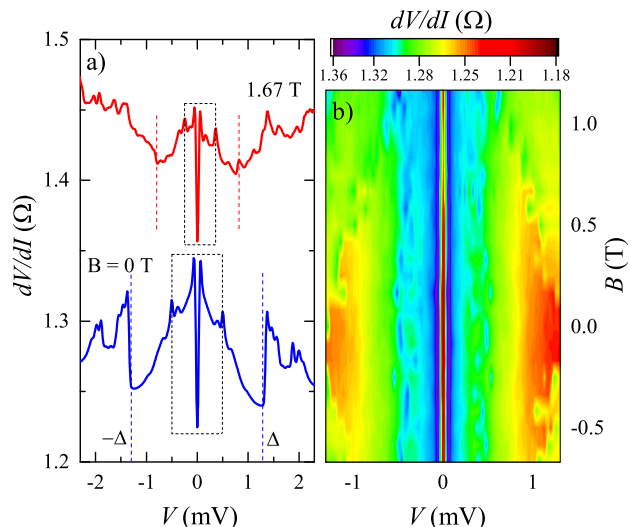


FIG. 4. (Color online) $dV/dI(V)$ characteristic for another Nb- $\text{Co}_3\text{Sn}_2\text{S}_2$ junctions. (a) $dV/dI(V)$ curves are measured at 30 mK for zero external magnetic field (blue) and for $B = 1.67$ T. The width of ZBA stays unaltered in high magnetic fields, while its height is slightly diminished. (b) Evolution of $dV/dI(V)$ characteristic in magnetic fields. The width of ZBA (green stripe around zero bias) is stable and independent of the sign of magnetic field.

disappears completely at higher temperatures, while the superconducting gap is still observable, see Fig. 2(b). Fig. 2(c) demonstrates the temperature dependence of the central structure region normalized width (the black rectangles) and ZBA normalized width (red diamonds). ZBA completely disappears at $T = 3.15$ K, while the wide subgap structure vanishes at about 3.5 K.

To investigate stability of ZBA against magnetic fields more precisely, we conducted two detailed measurements of $dV/dI(V)$ versus B at two temperatures - the minimal 30 mK and 1.4 K. The results are demonstrated as colormaps in Fig. 3(a,b). At both temperatures, the width and depth of ZBA are robust against magnetic fields. Suppression of ZBA starts only close to the critical field of the superconducting gap: after 3.3 T at 30 mK (Fig. 3(a)) and after 2.2 T at 1.4 K (Fig. 3(b)).

Qualitatively the same behavior is demonstrated by another Nb- $\text{Co}_3\text{Sn}_2\text{S}_2$ junction, demonstrating a larger interface scattering, see Fig. 4(a,b). The blue curve in Fig. 4(a) at zero magnetic field and 30 mK demonstrates a well-defined gap $\Delta = 1.3$ meV, denoted by the blue dashed lines, and a subgap structure with a sharp ZBA in the center. Again, ZBA is stable even in high magnetic fields, e.g., see the red curve at $B = 1.67$ T in Fig. 4(a). The colormap in Fig. 4(b) demonstrates stability of ZBA in moderate magnetic fields and its independence on the field's sign.

IV. DISCUSSION

Our main observation is the zero-bias anomaly, which is unusually robust over a wide range of the externally applied magnetic field and appears in the proximity-induced charge transport through the junctions involving the magnetic Weyl semimetal $\text{Co}_3\text{Sn}_2\text{S}_2$ connecting the superconducting Nb leads.

In our experiment, superconductivity is proximity induced in an interface vicinity of $\text{Co}_3\text{Sn}_2\text{S}_2$ WSM, which is characterized by the strong spin-orbit coupling and significant intrinsic Zeeman splitting. Note that the interface possesses an inhomogeneous structure, that could play an important constructive role in forming the magnetically stable ZBA. Similar situation was identified in the proximitized semiconductor nanowires virtually representing the one-dimensional systems and involving the spin-orbit coupling and the applied magnetic field producing the Zeeman splitting. The corresponding tunneling conductance characteristics have been progressively studied in such systems both experimentally³⁹⁻⁵⁰ and theoretically^{38,44,51-77}. In contrast to the semiconductor nanowire-based experiments, we observe ZBA in the proximitized magnetic Weyl semimetal, which is a three-dimensional sample in principle, while the corresponding chiral edge states reside in its two-dimensional surface. Fortunately, the applicability to two-dimensional systems of the main qualitative theoretical statements regarding the Majorana and Andreev states in one-dimensional case, is known to be usually justified^{9,12,73,75}. In addition, the problem could acquire some features of the one-dimensional character due to the anisotropy of the Fermi-arc surface transport and, possibly, the characteristic structure of surface termination. These allow us to use below some of those results for interpreting our experimental findings for ZBA in the Nb- $\text{Co}_3\text{Sn}_2\text{S}_2$ junctions.

A number of mechanisms resulting in ZBA in mesoscopic physics can be ruled out for our experiment. This in particular concerns the Oersted field-induced ZBA, when the circular Oersted field, exceeding the critical field H_c of a superconductor due to a large current density through an interface of a large area, leads to the current driven resistance peaks and ZBA^{78,79}. Such a possibility can be excluded since (i) ZBAs caused by the Oersted field are usually sensitive to an external magnetic field⁷⁸; (ii) ZBAs caused by the Oersted field exist almost till the superconductor's T_c ⁷⁸, in contrast to the temperature dependence in Fig. 2(c). Also, ZBAs in Fig. 2(a) and Fig. 4(a) cannot arise due to the Kondo effect, since they are symmetric and do not show a double-peak structure under the applied magnetic field^{78,80,81}. Furthermore, one should point out a possibility for the impurity-induced ZBA, which was actively studied with regard to semiconductor nanowires⁵⁴⁻⁶⁰. A detailed analysis has shown that disorder-induced ZBA is generally not so stable with varying strength of the Zeeman splitting⁵⁹, as compared to the experimental results in Figs. 3 and 4.

At the same time, there are a few possible scenarios re-

sulting in ZBA that yet cannot be excluded from the list of relevant physical mechanisms. In general, the topologically nontrivial zero-energy ABSs like Majorana bound states, localized at the surface of $\text{Co}_3\text{Sn}_2\text{S}_2$, could result in the prominent and magnetically stable ZBA being mainly robust with respect to disorder. An additional reason for ZBA to appear is known to be associated with the topologically trivial (non-Majorana) near-zero interfaced Andreev modes induced by the smooth inhomogeneities^{44,61–77}.

In particular, if there is a spatially inhomogeneous confining potential inside a proximitized nanowire, there are subgap ABSs. In the absence of the intrinsic Zeeman splitting as well as the external magnetic field, ABSs usually appear as two symmetric subgap conductance peaks. With increasing the external magnetic field in the presence of a strong spin-orbit coupling, ABSs can merge to form a single zero-energy state producing a single zero-bias conductance peak^{44,61–77}. Analogous effects can take place even for highly transparent contacts between a superconductor and a chiral channel⁶⁸.

Since the chiral edge states are topologically protected in WSM and topologically trivial and unprotected ABSs can be, to a certain extent, robust to disorder⁷⁶, a similar physical mechanism can be assumed to form zero-energy ABSs at the surface of $\text{Co}_3\text{Sn}_2\text{S}_2$ in proximity with a Nb superconductor.

(i) Although Weyl surface states are two-dimensional, they inherit the chiral property of the Chern insulator edge states, so a preferable direction is defined by Fermi arcs on a particular crystal surface.

(ii) The condition of a strong spin-orbit interaction is obviously satisfied for the $\text{Co}_3\text{Sn}_2\text{S}_2$ WSM²⁰. A sufficiently large intrinsic Zeeman splitting in the half-metallic $\text{Co}_3\text{Sn}_2\text{S}_2$ can be tuned by applying the external magnetic field. In the experiment, we observe no evidences of the finite-energy Andreev states, meaning that the inherent for the material Zeeman splitting substantially exceeds its critical value, above which the finite-

energy Andreev states coalesce together and form near-zero-energy midgap states.

(iii) An inhomogeneous potential is expected at the surface of $\text{Co}_3\text{Sn}_2\text{S}_2$, providing a platform for confined ABSs. After a mechanical cleavage, one expects to have multiple layer steps in the contact region for the Nb- $\text{Co}_3\text{Sn}_2\text{S}_2$ junctions. Cleavage mostly occurs between the Sn and S layers, but the topological surface states were revealed at the Sn layers^{23,82,83}. In addition, it has also been shown that there are Co_3Sn terraces at the surface of $\text{Co}_3\text{Sn}_2\text{S}_2$ ²⁴.

V. CONCLUSION

In conclusion, we have experimentally investigated charge transport through the interface between the Nb superconductor and magnetic WSM $\text{Co}_3\text{Sn}_2\text{S}_2$. Aside from Andreev reflection, we observe several additional features, among which the most notable is the prominent subgap ZBA, fairly stable against external magnetic fields up to the critical field of Nb. Possible mechanisms for magnetically stable ZBA to appear under the conditions studied should include the topological nature of WSM and its interfaces together with the effects of the strong spin-orbit coupling and large Zeeman splitting, which are intrinsic for the half-metallic WSM. As the promising scenario for ZBA observed in the transport measurements, we consider the proximity induced zero-energy ABSs interfacing between the superconducting Nb and $\text{Co}_3\text{Sn}_2\text{S}_2$.

ACKNOWLEDGMENTS

We wish to thank V.T. Dolgoplov for fruitful discussions, and S.V. Simonov for X-ray sample characterization. We gratefully acknowledge financial support partially by the RFBR (project No. 19-02-00203), RAS, and RF State task.

¹ A. A. Burkov and L. Balents, *Phys. Rev. Lett.* 107, 127205 (2011).

² For a review on topological semimetals, see N. P. Armitage, E. J. Mele, and A. Vishwanath, *Rev. Mod. Phys.* 90, 015001 (2018).

³ X. Wan, A. M. Turner, A. Vishwanath, S. Y. Savrasov, *Phys. Rev. B* 83, 205101 (2011).

⁴ A. A. Burkov, *Phys. Rev. Lett.* 113, 187202 (2014).

⁵ M. Breitzkreuz and P. W. Brouwer, *Phys. Rev. Lett.* 123, 066804 (2019).

⁶ A. F. Andreev, *Soviet Physics JETP* 19, 1228 (1964).

⁷ M. Tinkham, *Introduction to Superconductivity* (2d ed., McGrawHill, New York, 1996).

⁸ Y. Tanaka, M. Sato, and N. Nagaosa, *J. Phys. Soc. Jpn.* 81, 0111013 (2012).

⁹ M. Leijnse and K. Flensberg, *Semicond. Sci. Technol.* 27, 124003 (2012).

¹⁰ J. Alicea, *Rep. Prog. Phys.* 75, 076501 (2012).

¹¹ C. Beenakker, *Annu. Rev. Condens. Matter Phys.* 4, 113 (2013).

¹² M. Sato, S. Fujimoto, *J. Phys. Soc. Jpn.* 85, 072001 (2016).

¹³ J. Linder, A. V. Balatsky, *Rev. Mod. Phys.* 91, 045005 (2019).

¹⁴ T. Meng and L. Balents, *Phys. Rev. B* 86, 054504 (2012).

¹⁵ N. Bovenzi, M. Breitzkreuz, P. Baireuther, T. E. O'Brien, J. Tworzydo, I. Adagideli, and C. W. J. Beenakker, *Phys. Rev. B* 96, 035437 (2017).

¹⁶ Z. Farai and S. A. Jafari, *Phys. Rev. B* 100, 035447 (2019).

¹⁷ M. Hirschberger, S. Kushwaha, Z. Wang, Q. Gibson, S. Liang, C. A. Belvin, B. A. Bernevig, R. J. Cava, N. P.

- Ong, *Nat. Mater.* 15, 1161-1165 (2016).
- 18 G. Xu, H. Weng, Z. Wang, X. Dai, Z. Fang, *Phys. Rev. Lett.* 107, 186806 (2011).
 - 19 S. K. Kushwaha, Z. Wang, T. Kong, R. J. Cava, *J. Phys. Condens. Matter.* 30, 075701 (2018).
 - 20 E. Liu, Y. Sun, N. Kumar, L. Muechler, A. Sun, L. Jiao, S.-Y. Yang, D. Liu, A. Liang, Q. Xu, J. Kroder, V. Süß, H. Borrmann, C. Shekhar, Z. Wang, C. Xi, W. Wang, W. Schnelle, S. Wirth, Y. Chen, S. T. B. Goennenwein, and C. Felser, *Nat. Phys.* 14, 1125 (2018).
 - 21 Q. Wang, Y. Xu, R. Lou, Z. Liu, M. Li, Y. Huang, D. Shen, H. Weng, S. Wang, and H. Lei, *Nat. Commun.* 9, 3681 (2018).
 - 22 D. F. Liu, A. J. Liang, E. K. Liu, Q. N. Xu, Y. W. Li, C. Chen, D. Pei, W. J. Shi, S. K. Mo, P. Dudin, T. Kim, C. Cacho, G. Li, Y. Sun, L. X. Yang, Z. K. Liu, S. S. P. Parkin, C. Felser, Y. L. Chen, *Science*, Vol. 365, Issue 6459, pp. 1282-1285 (2019).
 - 23 N. Morali, R. Batabyal, P. K. Nag, E. Liu, Q. Xu, Y. Sun, B. Yan, C. Felser, N. Avraham, and H. Beidenkopf, *Science* 365, 1286 (2019).
 - 24 S. Howard, L. Jiao, Z. Wang, P. Vir, C. Shekhar, C. Felser, T. Hughes, V. Madhavan, arXiv:1910.11205 (2019).
 - 25 A. Kononov, O. O. Shvetsov, S. V. Egorov, A. V. Timonina, N. N. Kolesnikov and E. V. Deviatov, *EPL*, 122, 27004 (2018).
 - 26 O. O. Shvetsov, V. D. Esin, A. V. Timonina, N. N. Kolesnikov, and E. V. Deviatov, *Phys. Rev. B* 99, 125305 (2019).
 - 27 O. O. Shvetsov, V. D. Esin, A. V. Timonina, N. N. Kolesnikov and E. V. Deviatov, *EPL*, 127, 57002 (2019).
 - 28 S. Bouvron, M. Stokmaier, M. Marz, and G. Goll, *Low Temp. Phys.* 39, 274 (2013).
 - 29 T. Tokuyasu, J. A. Sauls, D. Rainer, *Phys. Rev. B* 38, 8823 (1988).
 - 30 J. A. Ouassou, A. Pal, M. Blamire, M. Eschrig, and J. Linder, *Sci. Rep.* 7, 1932 (2017).
 - 31 O. O. Shvetsov, V. D. Esin, Yu. S. Barash, A. V. Timonina, N. N. Kolesnikov, and E. V. Deviatov, *Phys. Rev. B* 101, 035304 (2020).
 - 32 O. O. Shvetsov, V. A. Kostarev, A. Kononov, V. A. Golyashov, K. A. Kokh, O. E. Tereshchenko, and E. V. Deviatov, *EPL* 119, 57009 (2017).
 - 33 W. J. Tomasch, *Phys. Rev. Lett.* 16, 16 (1966).
 - 34 W. L. McMillan, P. W. Anderson, *Phys. Rev. Lett.* 16, 85 (1966).
 - 35 D. R. Heslinga, S. E. Shafranjuk, H. van Kempen, and T. M. Klapwijk, *Phys. Rev. B* 49, 10484 (1994).
 - 36 J. Wiedenmann, E. Liebhaber, J. Kbert, E. Bocquillon, Ch. Ames, H. Buhmann, T. M. Klapwijk, and L. W. Molenkamp, *Phys. Rev. B* 96, 165302 (2017).
 - 37 A. Kononov, V. A. Kostarev, B. R. Semyagin, V. V. Preobrazhenskii, M. A. Putyato, E. A. Emelyanov, and E. V. Deviatov, *Phys. Rev. B* 96, 245304 (2017).
 - 38 So Takei, B. M. Fregoso, Hoi-Yin Hui, A. M. Lobos, and S. Das Sarma, *Phys. Rev. Lett.* 110, 186803 (2013).
 - 39 V. Mourik, K. Zuo, S. M. Frolov, S. R. Plissard, E. P. A. M. Bakkers, L. P. Kouwenhoven, *Science* 336, 1003 (2012).
 - 40 A. Das, Y. Ronen, Y. Most, Y. Oreg, M. Heiblum, and H. Shtrikman, *Nat. Phys.* 8, 887 (2012).
 - 41 M. T. Deng, C. L. Yu, G. Y. Huang, M. Larsson, P. Caroff, and H. Q. Xu, *Nano Lett.* 12, 6414 (2012).
 - 42 W. Chang, S. M. Albrecht, T. S. Jespersen, F. Kuemmeth, P. Krogstrup, J. Nygård, and C. M. Marcus, *Nanotech.* 10, 232 (2015).
 - 43 S. M. Albrecht, A. P. Higginbotham, M. Madsen, F. Kuemmeth, T. S. Jespersen, J. Nygård, P. Krogstrup, and C. M. Marcus, *Nature* 531, 206 (2016).
 - 44 M. T. Deng, S. Vaitieknas, E. B. Hansen, J. Danon, M. Leijnse, K. Flensberg, J. Nygård, P. Krogstrup, C. M. Marcus, *Science* 354, 1557 (2016).
 - 45 J. Chen, P. Yu, J. Stenger, M. Hocevar, D. Car, S. R. Plissard, E. P. A. M. Bakkers, T. D. Stanescu, S. M. Frolov, *Sci. Adv.* 3, e1701476 (2017).
 - 46 Ö. Gül, H. Zhang, F. K. de Vries, J. van Veen, K. Zuo, V. Mourik, S. Conesa-Boj, M. P. Novak, D. J. van Woerkom, M. Quinetto-Perez, M. C. Cassidy, A. Geresdi, S. Koelling, D. Car, S. R. Plissard, E. P. A. M. Bakkers, and L. P. Kouwenhoven, *Nano Lett.* 17, 2690 (2017).
 - 47 H. Zhang, Ö. Gül, S. Conesa-Boj, M. P. Novak, M. Wimmer, K. Zuo, V. Mourik, F. K. de Vries, J. van Veen, M. W. A. de Moor, J. D. S. Bommer, D. J. van Woerkom, D. Car, S. R. Plissard, E. P. A. M. Bakkers, M. Quinetto-Perez, M. C. Cassidy, S. Koelling, S. Goswami, K. Watanabe, T. Taniguchi, and L. P. Kouwenhoven, *Nat. Comm.* 8, 16025 (2017).
 - 48 Ö. Gül, H. Zhang, J. D. S. Bommer, M. W. A. de Moor, D. Car, S. R. Plissard, E. P. A. M. Bakkers, A. Geresdi, K. Watanabe, T. Taniguchi, and L. P. Kouwenhoven, *Nat. Nanotech.* 13, 192 (2018).
 - 49 A. Grivnin, E. Bor, M. Heiblum, Y. Oreg, and H. Shtrikman, *Nat. Com.* 10, 1940 (2019).
 - 50 J. Chen, B. D. Woods, P. Yu, M. Hocevar, D. Car, S. R. Plissard, E. P. A. M. Bakkers, T. D. Stanescu, and S. M. Frolov, *Phys. Rev. Lett.* 123, 107703 (2019).
 - 51 R. M. Lutchyn, J. D. Sau, S. Das Sarma, *Phys. Rev. Lett.* 105, 077001 (2010).
 - 52 Y. Oreg, G. Refael, and F. von Oppen, *Phys. Rev. Lett.* 105, 177002 (2010).
 - 53 E. J. H. Lee, X. Jiang, R. Aguado, G. Katsaros, C. M. Lieber, and S. De Franceschi, *Phys. Rev. Lett.* 109, 186802 (2012).
 - 54 D. Bagrets and A. Altland, 109, 227005 (2012).
 - 55 W. DeGottardi, D. Sen, and S. Vishveshwara, *Phys. Rev. Lett.* 110, 146404 (2013).
 - 56 W. DeGottardi, M. Thakurathi, S. Vishveshwara, and D. Sen, *Phys. Rev. B* 88, 165111 (2013).
 - 57 J. Liu, A. C. Potter, K. T. Law, and P. A. Lee, *Phys. Rev. Lett.* 109, 267002 (2012).
 - 58 D. I. Pikulin, J. P. Dahlhaus, M. Wimmer, H. Schomerus and C. W. J. Beenakker, *New J. Phys.* 14, 125011 (2012).
 - 59 D. Rainis, L. Trifunovic, J. Klinovaja, and D. Loss, *Phys. Rev. B* 87, 024515 (2013).
 - 60 İ. Adagideli, M. Wimmer, and A. Teker, *Phys. Rev. B* 89, 144506 (2014).
 - 61 D. Chevallier, D. Sticlet, P. Simon, and C. Bena, *Phys. Rev. B* 85, 235307 (2012).
 - 62 G. Kells, D. Meidan, and P. W. Brouwer, *Phys. Rev. B* 86, 100503 (2012).
 - 63 E. Prada, P. San-Jose, and R. Aguado, *Phys. Rev. B* 86, 180503 (2012).
 - 64 D. Roy, N. Bondyopadhyaya, and S. Tewari, *Phys. Rev. B* 88, 020502 (2013).
 - 65 E. J. H. Lee, X. Jiang, M. Houzet, R. Aguado, C. M. Lieber, and S. De Franceschi, *Nat. Nanotech.* 9, 79 (2014).
 - 66 T. D. Stanescu, and S. Tewari, *Phys. Rev. B* 89, 220507 (2014).

- ⁶⁷ J. Klinovaja, and D. Loss, *Eur. Phys. J. B* 88, 62 (2015).
- ⁶⁸ P. San-Jose, J. Cayao, E. Prada, R. Aguado, *Sci. Rep.* 6, 21427 (2016).
- ⁶⁹ C.-X. Liu, J. D. Sau, T. D. Stanescu, and S. Das Sarma, *Phys. Rev. B* 96, 075161 (2017).
- ⁷⁰ C. Fleckenstein, F. Domínguez, N. T. Ziani, and B. Trauzettel, *Phys. Rev. B* 97, 155425 (2018).
- ⁷¹ C. Moore, T. D. Stanescu, and S. Tewari, *Phys. Rev. B* 97, 165302 (2018).
- ⁷² C. Reeg, O. Dmytruk, D. Chevallier, D. Loss, and J. Klinovaja, *Phys. Rev. B* 98, 245407 (2018).
- ⁷³ A. Vuik, B. Nijholt, A. R. Akhmerov and M. Wimmer, *SciPost Phys.* 7, 061 (2019).
- ⁷⁴ Y-H. Lai, J. D. Sau, and S. Das Sarma, *Phys. Rev. B* 100, 045302 (2019).
- ⁷⁵ B. D. Woods, J. Chen, S. M. Frolov, and T. D. Stanescu, *Phys. Rev. B* 100, 125407 (2019).
- ⁷⁶ T. D. Stanescu and S. Tewari, *Phys. Rev. B* 100, 155429 (2019).
- ⁷⁷ B. D. Woods, S. Das Sarma, and T. D. Stanescu, *Phys. Rev. B* 101, 045405 (2020).
- ⁷⁸ J. A. Gifford, G. J. Zhao, B. C. Li, J. Zhang, D. R. Kim, T. Y. Chen, *J. Appl. Phys.*, 120(16), 163901 (2016).
- ⁷⁹ G. Sheet, S. Mukhopadhyay, and P. Raychaudhuri, *Phys. Rev. B* 69, 134507 (2004).
- ⁸⁰ S. M. Cronenwett, H. J. Lynch, D. Goldhaber-Gordon, L. P. Kouwenhoven, C. M. Marcus, K. Hirose, N. S. Wingreen, and V. Umansky, *Phys. Rev. Lett.* 88, 226805 (2002).
- ⁸¹ A. A. Clerk, V. Ambegaokar, and S. Hershfield, *Phys. Rev. B* 61, 3555 (2000).
- ⁸² J.-X. Yin, S. S. Zhang, G. Chang, Q. Wang, S. S. Tsirkin, Z. Guguchia, B. Lian, H. Zhou, K. Jiang, I. Belopolski, N. Shumiya, D. Multer, M. Litskevich, T. A. Cochran, H. Lin, Z. Wang, T. Neupert, S. Jia, H. Lei, and M. Z. Hasan, *Nat. Phys.* 15, 443 (2019).
- ⁸³ L. Muechler, E. Liu, Q. Xu, C. Felser, Y. Sun, *arXiv:1712.08115* (2017).